*DOI:*
10.1021/acs.langmuir.9b03130

*Document Version*
Peer reviewed version

# Structure and dynamics of nanoconfined water between surfactant monolayers

Robert M. Ziolek,[†] Franca Fraternali,[‡] Ali Dhinojwala,[¶] Mesfin Tsige,[¶] and Christian D. Lorenz[*,†]

†*Biological Physics and Soft Matter Group, Department of Physics, King's College London, London, WC2R 2LS, UK*

‡*Randall Division of Cell and Molecular Biophysics, King's College London, London, SE1 1UL, UK*

¶*College of Polymer Science and Polymer Engineering, The University of Akron, Akron, Ohio 44325, USA*

E-mail: chris.lorenz@kcl.ac.uk

**Abstract**

The properties of nanoconfined water arise in direct response to the properties of the interfaces that confine it. A great deal of research has focused on understanding how and why the physical properties of confined water differ greatly from the bulk. In this work, we have used all-atom molecular dynamics (MD) simulations to provide a detailed description of the structural and dynamical properties of nanoconfined water between two monolayers consisting of an archetypal ionic surfactant, cetrimonium bromide (CTAB, $[CH_3(CH_2)_{15}N(CH_3)_3]^+$ $Br^-$). Small differences in the area per surfactant of the monolayers impart a clear effect on the intrinsic density, mobility and ordering of the interfacial water layer confined by the monolayers. We find that as the area per surfactant within a monolayer decreases, the mobility of the interfacial

water molecules decreases in response. As the monolayer packing density decreases, we find that each individual CTAB molecule has a greater effect on the ordering of water molecules in its first hydration shell. In a denser monolayer, we observe that the effect of individual CTAB molecules on the ordering of water molecules is hindered by increased competition between headgroups. Therefore, when two monolayers with different areas per surfactant are used to confine a nanoscale water layer, we observe the emergence of non-centrosymmetry.

# Introduction

The nature of confined water and the properties of the interfaces that confine it are intimately linked. Confinement affects the structure and dynamics of water through interactions between water and the interfaces of its confinement matrix.[1–4] The physical properties of confined water are strongly dependent on the thickness of the confined layer and the structure of the confining interfaces.[5] The desire to understand the origins of the difference in the physical properties of confined water as compared to its bulk properties has led to a significant amount of research.[6–19]

Surfactant-covered aqueous interfaces are ubiquitous in everyday life. These interfaces play a key role in various commercial products, where surfactants adsorb onto the surface of bubbles or oil droplets to stabilize foams and emulsions. Examples of such foams and emulsions are commonly found in chemical products, pharmaceuticals, nutritional supplements, detergents, cosmetics, and lubricants.[20–31] In a majority of these applications, the ability of surfactants to adsorb to a liquid interface and then encapsulate water in nanoscale environments play a key role. Therefore understanding the properties of water confined between surfactant interfaces has significant relevance to these industrial products.

In this manuscript, we have used all-atom molecular dynamics (MD) simulations to investigate the structural and dynamical properties of nanoconfined water between two monolayers consisting of an archetypal ionic surfactant, cetrimonium bromide ($[CH_3(CH_2)_{15}N(CH_3)_3]^+$

$Br^-$), which we refer to here as CTAB. Previous studies have investigated the structure of water near the interface of a CTAB monolayer through experiments[32–37] and MD simulations.[19,34,38] However, it was only recently that Dhopatkar and co-workers studied a thin layer of water under confinement by two CTAB monolayers using sum-frequency generation (SFG) spectroscopy.[9] They commented on the intricate ordering of the confined water layer, akin to that found in ice. Unexpectedly, their centrosymmetry-sensitive sum-frequency generation (SFG) spectroscopic experiments indicated a breakdown in the symmetry of the confined water layer, despite the two monolayers confining the water layer both being made up of CTAB.

In this manuscript, we present an MD simulation study of water nanoconfined between two CTAB monolayers with subtly different packing densities. By modeling the monolayer-water interface using an intrinsic surface description, we determine how the structure and dynamics of the nanoconfined water layer are affected by the structure of the monolayers themselves. In doing so, we explore the emergence of non-centrosymmetry in the confined water layer.

# Methods

## Simulation details

Four model systems have been simulated using all-atom classical molecular dynamics. Each system consists of an approximately 3 nm thick layer of water confined between two CTAB monolayers as depicted in Figure 1(a). Two symmetric systems have been simulated, where both the upper and lower monolayers have the same lateral area per CTAB molecule ($A_{\mathrm{CTAB}}$): one system with $A_{\mathrm{CTAB}} = 52$ Å$^2$ (SYM52) and a second system with $A_{\mathrm{CTAB}} = 49$ Å$^2$ (SYM49). Two asymmetric systems have also been simulated. The first (ASYM) has one monolayer with $A_{\mathrm{CTAB}} = 52$ Å$^2$ and the other monolayer has $A_{\mathrm{CTAB}} = 49$ Å$^2$. The second asymmetric system (ASYM2) has one monolayer with $A_{\mathrm{CTAB}} = 55$ Å$^2$ and the other

monolayer has $A_{\mathrm{CTAB}} = 49$ Å$^2$. The areas per surfactant of these systems were chosen with reference to the average values determined experimentally by Dhopatkar *et al.*[9] Additionally, a single monolayer system (MONO) with $A_{\mathrm{CTAB}} = 49$ Å$^2$ and 21600 water molecules (a water layer of approximately 6 nm) has been simulated for comparison with the confined systems. Further details of the five simulated systems are summarized in Table 1.

Table 1: Details of the simulated systems. ML1 and ML2 refer to the two monolayers. $n_{\mathrm{CTAB}}$ refers to the number of CTAB molecules, $n_{\mathrm{H_2O}}$ the number of water molecules, and $n_{\mathrm{atoms}}$ to the total number of atoms in the simulated system.

| System | $n_{\mathrm{CTAB}}$ (ML1) | $n_{\mathrm{CTAB}}$ (ML2) | $n_{\mathrm{H_2O}}$ | $n_{\mathrm{atoms}}$ |
|---|---|---|---|---|
| SYM49 | 212 | 212 | 10400 | 57912 |
| SYM52 | 200 | 200 | 10400 | 56400 |
| ASYM | 212 | 200 | 10400 | 57156 |
| ASYM2 | 212 | 188 | 10400 | 56400 |
| MONO | 212 | - | 21600 | 76956 |

CTAB was parameterized with the CHARMM36 forcefield using CGenFF.[39,40] Water was treated with the CHARMM-modified TIP3P water model,[41] which is the water model used in the parameterization of the CHARMM36 forcefield[42,43] and which has been employed in various previous MD simulations of confined water.[6,44,45] Parameters for the bromide counter-anion were taken from Horinek *et al*[46] however no excess salt was included in the simulations. Initial configurations of each system were built using Packmol.[47] The simulation boxes (all with dimensions of $101.9 \times 101.9 \times 100$ Å$^3$) are periodic in the $xy$-plane but not in the $z$-direction; any molecules that diffuse to the maximum extents of the simulation box in the $z$-dimension are reflected back towards the monolayer system. All of the simulations were performed with the LAMMPS molecular dynamics simulation engine.[48] Energy minimization by steepest descent (with energy tolerance of $10^{-4}$ kcal mol$^{-1}$ and force tolerance of $10^{-6}$ kcal mol$^{-1}$ Å$^{-1}$) was first used to eliminate high-energy steric artefacts induced when creating the systems. In order to maintain the well-defined $A_{\mathrm{CTAB}}$ values, both equilibration and production simulations were performed in the canonical (NVT) ensemble[49]

at 300 K using the Nosé-Hoover thermostat. Bonds and angles containing hydrogen were constrained using the SHAKE algorithm[50] in order to use a timestep of 2 fs. In both the equilibration and production simulations, the van der Waals and Coulomb interaction cut-off distances were set to 12 Å. The monolayer roughness, the width of the confined water layer, and the orientation of CTAB molecules indicated rapid equilibration of the system within a few nanoseconds. The production simulations were run for 200 ns; the final 150 ns of the trajectories was used for the analyses presented in this work.

## Analysis methods

Throughout the remainder of this manuscript, we present the results of the various analyses for the SYM52 and ASYM2 systems. The results for the other systems are presented in the Supplementary Information and discussed in the manuscript. Unless noted otherwise, all trends that are mentioned are observed in all systems. All data analysis was performed using Python code developed in-house, which makes use of the MDAnalysis package.[51] The visualizations were produced using VMD.[52]

### Intrinsic surface of the monolayer-water interface

Figures 1(a) and (b) highlight the roughness and patchiness of the CTAB monolayers, as previously observed in studies of CTAB monolayers at the air-water interface.[19,34] These two characteristics present a challenge when analyzing the structure of the confined water layer: two water molecules at the same position in the $z$-dimension can experience entirely different physical environments. One water molecule at a given $z$-position may be surrounded by other water molecules in the water layer, away from the monolayer interface, while another at the same $z$-dimension may have diffused past the CTAB headgroups into the hydrocarbon tail region of the surfactants, or be at the air-water interface, given the rough and patchy nature of the monolayers.

In order to faithfully describe the confined water at the interface with the monolayers,

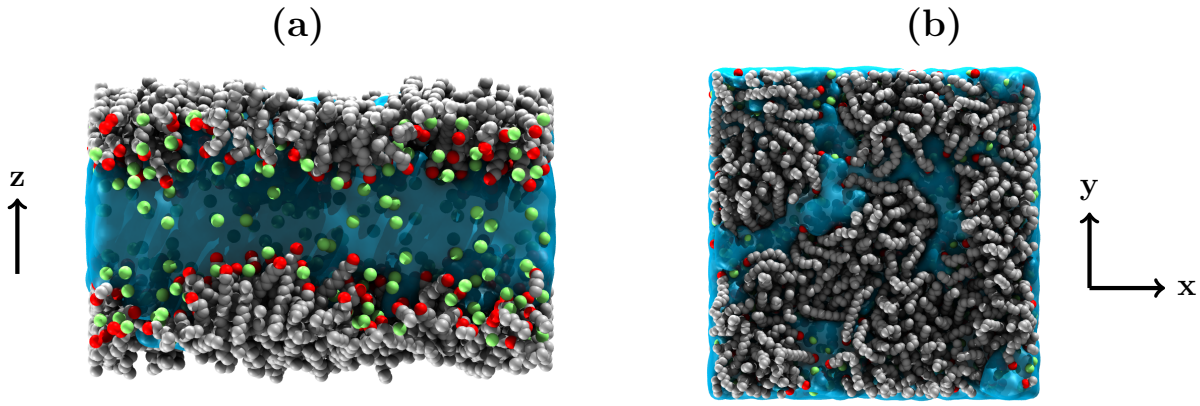


Figure 1: (a) Side projection and (b) top projection of ASYM system at equilibrium. Note the roughness of the monolayers (a) and patchy domain structures they form (b). Carbon atoms are colored gray, nitrogen red, bromide anions green and water is represented as the continuous blue surface. Hydrogen atoms and terminal onium methyl groups not shown for clarity.

discretized intrinsic surfaces were defined at the monolayer-water interfaces, using a $40 \times 40$ grid corresponding to lateral resolution of approximately $2.6 \times 2.6$ Å$^2$. This grid resolution, which is approximately the size of a single water molecule, provides a suitable description of the monolayer-water interface. A characteristic interfacial peak in the water density is clearly observable and the water density decays monotonically at the air-water interface (see SI Fig. 5(c) and (d)). The lateral resolution of the surfaces is an order of magnitude less than the area per surfactant values of the CTAB monolayers, meaning that we characterize the surface in sufficient detail. As we show in the supplementary information (SI Fig. 1), using a much finer $60 \times 60$ grid does not correctly partition the monolayer-water and air-water interfaces, showing a physically unrealistic decay of the intrinsic water density at the air-water interface. A significantly coarser grid, such as a $20 \times 20$ grid, does not encapsulate the roughness of the monolayer-water interface in sufficient detail and does not partition monolayer-water and air-water interfacial contributions.

We chose to develop this bespoke intrinsic surface method, rather than using a method employing specific surfactant headgroup atoms as anchor points[53] or a probe-based method[54], since it allows us to naturally partition the intrinsic surface into the monolayer-water and

air-water interfaces. Viewing either monolayer from the middle of the confined layer, the $z$-position of the monolayer-water intrinsic surface is defined for each grid box as the CTAB atom found protruding furthest into the confined water layer in that given grid box. If no CTAB atom in the monolayer is found (in gaps between the monolayer domains), then the average $z$-position of the 8 adjacent grid boxes is used instead, iterating until the whole interface is described. The intrinsic density of the water layer is then written as

$$\tilde{\rho}(z) \equiv \frac{1}{A_{IS}} \left\langle \sum_i \delta[z - (z_i - \xi(x,y))] \right\rangle \tag{1}$$

where $z_i$ is the $z$-position of the oxygen atom of water molecule $i$, $\xi(x,y)$ is the $z$-position of the intrinsic surface, and $A_{IS}$ is the lateral area of the intrinsic surface.

### Monolayer structural properties

We define monolayer roughness $\mathrm{ML}_{\mathrm{roughness}}$ as the average standard deviation of the $z$-positions of the headgroup nitrogen atoms. The average CTAB tilt angle, $\theta_{\mathrm{tilt}}^{\mathrm{CTAB}}$, is the angle formed by the vector connecting the onium nitrogen atom in the headgroup to the terminal carbon in the alkyl chain with respect to the $xy$-plane. A value of $\theta_{\mathrm{tilt}}^{\mathrm{CTAB}} = 0°$ corresponds to a CTAB molecule lying flat along the water-monolayer interface, and $\theta_{\mathrm{tilt}}^{\mathrm{CTAB}} = 90°$ corresponds to a CTAB molecule oriented along the monolayer normal, with its headgroup interacting with the confined water layer. The fraction of the intrinsic surface actually covered by CTAB molecules, $\mathrm{ML}_{\mathrm{coverage}}$, is found using the partitioning of the intrinsic surfaces into air-water and monolayer-water contributions described previously.

### Dynamics of the confined water molecules

We consider the van Hove self-correlation function (VHSCF) of water molecules, with a lag time of $\tau = 20$ ps, as a measure of the mobility of water. The intrinsic VHSCF profile, $\tilde{G}_s(z,\tau)$, of the confined water layer is calculated as

$$\tilde{G}_s(z,\tau) \equiv \left\langle \sum_i |\mathbf{r}_i(t+\tau) - \mathbf{r}_i(t)| \delta[z - (z_i - \xi(x,y,t))] \right\rangle . \quad (2)$$

Here $\mathbf{r}_i(t)$ is the position of a given water oxygen atom at time $t$. Using this description, rather than time-averaged diffusion coefficients, provides detailed spatial resolution as a function of $z$.

**Hydrogen bonding in confined water**

The number of hydrogen bonds that a water molecule forms is referred to as its degree of hydrogen bonding. We calculate the intrinsic average hydrogen bonding degree profile, $\tilde{n}_{\mathrm{HB}}$, as

$$\tilde{n}_{\mathrm{HB}}(z) \equiv \left\langle \sum_i n_{\mathrm{HB},i}\, \delta[z - (z_i - \xi(x,y))] \right\rangle , \quad (3)$$

where $n_{\mathrm{HB},i}$ is the degree of hydrogen bonding of water molecule $i$ at a given time. The geometric criteria used to determine whether two water molecules are hydrogen-bonded are $r_{\mathrm{OH}} < 2.45$ Å, $r_{\mathrm{OO}} < 3.60$ Å and $\theta_{\mathrm{OHO}} < 120°$. Here, $r_{\mathrm{OH}}$ is the distance between the donor-hydrogen and acceptor-oxygen, $r_{\mathrm{OO}}$ is the distance between the acceptor-oxygen and donor-oxygen, and $\theta_{\mathrm{OHO}}$ is the angle between the vectors connecting the donor-hydrogen and acceptor-oxygen, and the donor-oxygen and acceptor-oxygen. These cutoff distances correspond to the position of the first minimum in the respective pair distribution functions (SI Fig. 2(e) and (f)).

**Intrinsic orientational distribution of water molecules**

The orientation of the water molecules is described by the angle between the $z$ unit vector ($\hat{\mathbf{z}}$, normal to the monolayer planes) and the normalized vector that bisects the water bond angle $\hat{\mathbf{r}}_i = (\mathbf{r}_{\mathrm{OH}_1} + \mathbf{r}_{\mathrm{OH}_2})/(|\mathbf{r}_{\mathrm{OH}_1} + \mathbf{r}_{\mathrm{OH}_2}|)$ (see SI Fig. 3), as used in previous studies.[8,55] The intrinsic density-weighted orientational distribution is then calculated as

$$\tilde{\Gamma}^{(1)}(z) \equiv \frac{1}{A_{IS}} \left\langle \sum_i \hat{\mathbf{z}} \cdot \hat{\mathbf{r}}_i \, \delta[z - (z_i - \xi(x,y))] \right\rangle, \tag{4}$$

while the second moment, which describes whether water molecules on average lie in the $xy$-plane ($\tilde{\Gamma}^{(2)} < 0$) or orthogonal to it ($\tilde{\Gamma}^{(2)} > 0$), is given as

$$\tilde{\Gamma}^{(2)}(z) \equiv \frac{1}{A_{IS}} \left\langle \sum_i \frac{3(\hat{\mathbf{z}} \cdot \hat{\mathbf{r}}_i)^2 - 1}{2} \delta[z - (z_i - \xi(x,y))] \right\rangle. \tag{5}$$

**Monolayer environment effects on the confined water molecules**

We quantify the effects of local environment on the orientation of confined water molecules by using the coordination numbers of different atoms. The pair distribution function of two atomic species, $a$ and $b$, is defined as

$$g(r)_{a,b} = \frac{\rho(r)_{a,b}}{\langle \rho_b \rangle}, \tag{6}$$

where $\rho(r)_{a,b}$ is the density of atom species $b$ at a distance $r$ from atom species $a$, and $\langle \rho_b \rangle$ is the average density of type $b$ atoms. The coordination number of $b$ around $a$ is then usually defined as $n(r_{\min})_{a,b} = 4\pi \int_0^{\mathrm{r_{min}}} \mathrm{d}r \, r^2 g(r)_{a,b}$, where $r_{\min}$ is the distance at which the first minimum occurs in the pair distribution function. In the case of the onium-onium pair distribution function, $g(r)_{\mathrm{N^+,N^+}}$, the inherent disorder of the monolayers is reflected in its complex features, with a point of inflection at $r = 7.5$ Å and a large value of $r_{\min} = 12.6$ Å (see SI Fig. 2(a)). Therefore, to ensure that the coordination number describes only the local environment of CTAB headgroups, we define the inter-headgroup coordination number $n(r_{\max})_{\mathrm{N^+,N^+}} = 4\pi \int_0^{\mathrm{r_{max}}} \mathrm{d}r \, r^2 g(r)_{a,b}$, where $r_{\max} = 8.3$ Å is the distance at which the global maximum occurs in the pair distribution function (most probable inter-headgroup distance). The positions of the first minimum and global maximum of each pair distribution function are the same over the $A_{\mathrm{CTAB}}$ range considered in this work. We use the $r_{\max}$ value of the onium-onium pair distribution function to calculate the probability distribution of the inter-

headgroup coordination number $p(n_{\mathrm{N^+,N^+}})$. This is found by evaluating the number of other headgroup onium atoms within the distance $r_{\max}$ from each headgroup onium atom in turn.

# Results and discussion

## Equilibrium properties of the CTAB monolayers

The physical characteristics of the CTAB monolayers in the different systems are detailed in Table 2. The average tilt angle of the CTAB molecules increases (i.e. CTAB molecules are more vertically orientated with respect to the water layer) with decreasing $A_{\mathrm{CTAB}}$ (increased packing density). The range of $\theta_{\mathrm{tilt}}^{\mathrm{CTAB}}$ values determined here are lower than those determined experimentally.[9] This finding is consistent with the work of Yazhgur and co-workers: they have shown that CTAB monolayers are disordered, with a significant portion lying in the plane of the monolayer-water interface even at higher packing densities than those considered in this work.[34] The monolayer roughness also increases with decreasing $A_{\mathrm{CTAB}}$ (increased packing density). There are clear differences between the roughness of the monolayers in the two asymmetric systems, most notably in ASYM2, in which the difference in $A_{\mathrm{CTAB}}$ of the two monolayers is greater. In the symmetric systems, the roughness of the two monolayers is approximately the same. The fraction of the water surface area identified as being covered by each CTAB monolayer increases from 0.88 to 0.90 with increasing monolayer density. There are no freely solvated CTAB molecules at equilibrium and CTAB molecules do not diffuse between the monolayers during the simulations. The average thickness of the confined water layer is approximately the same for all four confined systems (between 2.97 and 3.00 nm). This was calculated by evaluating the average volume encompassed between the two intrinsic surfaces over the course of the simulation and dividing by the (fixed) lateral surface area.

SI Figure 4 shows the probability distribution of inter-headgroup onium-onium coordination number in SYM52 and ASYM2. As packing density decreases ($A_{\mathrm{CTAB}}$ increases), lower values of the inter-headgroup coordination number ($n_{\mathrm{N^+,N^+}}$) increase in probability while

Table 2: Equilibrium physical properties of the CTAB monolayers: the average angle of CTAB molecules with respect to the monolayer plane ($\theta_{\text{tilt}}^{\text{CTAB}}$), the roughness of monolayers ($\text{ML}_{\text{roughness}}$) and the fraction of the total water-monolayer interface covered by the monolayer domains ($\text{ML}_{\text{coverage}}$). The uncertainty in the mean values of $\theta_{\text{tilt}}^{\text{CTAB}}$ reported here is described by their standard errors, which is $0.02\,^{\circ}$ in all cases. The range of $\text{ML}_{\text{roughness}}$ and $\text{ML}_{\text{coverage}}$ values are described by their standard deviations, which are 0.3 Å and 0.01 respectively for all values reported. The $A_{\text{CTAB}}$ values are included for reference.

| System | $A_{\text{CTAB}}$ [Å$^2$] | | $\theta_{\text{tilt}}^{\text{CTAB}}$ [$^o$] | | $\text{ML}_{\text{roughness}}$ [Å] | | $\text{ML}_{\text{coverage}}$ | |
|---|---|---|---|---|---|---|---|---|
| | ML1 | ML2 | ML1 | ML2 | ML1 | ML2 | ML1 | ML2 |
| SYM49 | 49 | 49 | 46.5 | 46.5 | 5.1 | 5.1 | 0.90 | 0.90 |
| SYM52 | 52 | 52 | 45.4 | 45.3 | 4.7 | 4.8 | 0.89 | 0.89 |
| ASYM | 52 | 49 | 45.5 | 46.2 | 4.7 | 5.1 | 0.89 | 0.90 |
| ASYM2 | 55 | 49 | 44.1 | 46.2 | 4.4 | 5.1 | 0.88 | 0.90 |

higher values of $n_{\text{N}^+,\text{N}^+}$ decrease. Even for small differences in $A_{\text{CTAB}}$, there are quantifiable differences in the structure of the monolayers.

## Intrinsic density of the confined water

The interfacial density of water in the SYM52 and ASYM2 systems, as found using the intrinsic surface approach previously described, is shown in Figure 2. In this section, and elsewhere, profiles with respect to both monolayers in the SYM52 system are both shown overlaid. The instantaneous monolayer-water interface is defined at $z = 0$. Values of $z > 0$ correspond to the space taken up by the confined water layer between the two monolayers, and values of $z < 0$ refer to the region of space 'above' the interface, where the alkyl tails of the surfactants are found. We use this definition for both interfaces, such that the distributions can be overlaid to allow straightforward comparison.

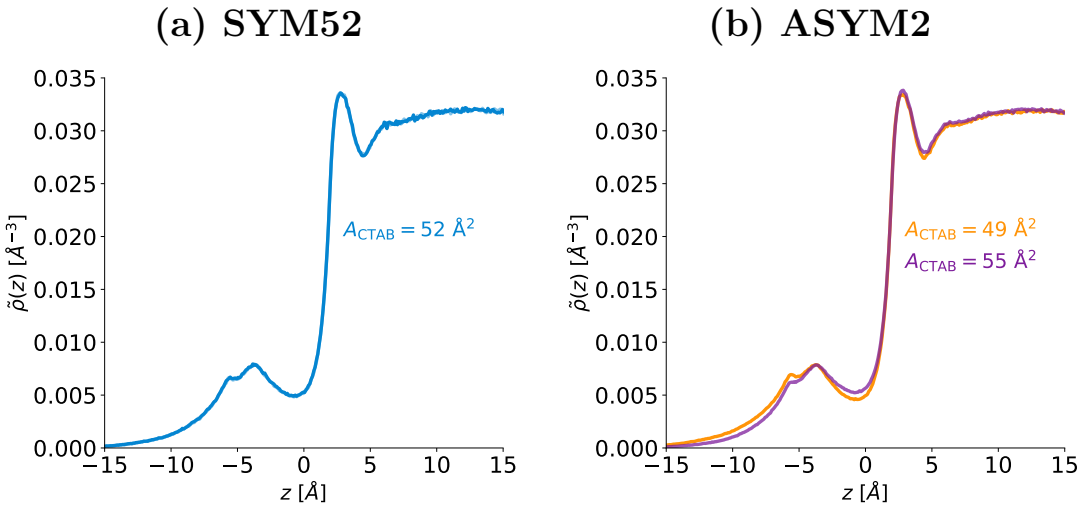


Figure 2: Intrinsic density of water in (a) SYM52 and (b) ASYM2. The results for the other confined systems can be found in SI Fig. 5(a) and (b). Note that in (a), results with respect to both monolayers are shown, which almost perfectly overlap.

We see that both systems in Figure 2 show broadly similar intrinsic density profiles, as expected, given the small differences in the area per surfactant ($A_{\mathrm{CTAB}}$) between the studied monolayers. In all systems, we observe a peak in the intrinsic density close to the monolayer interface at $z = 2.85$ Å. This indicates that water molecules are highly ordered close to the interface due to attractive electrostatic interactions between the cationic monolayer headgroups and the polar water oxygen atoms. Numerous studies of hydrophilic sodium dodecyl sulphate (SDS) surfactant monolayers at the air/water interface have revealed multiple peaks in the intrinsic density of water.[55–57] Bekele and Tsige have recently shown that there are also multiple peaks in the density of water close to a polystyrene surface.[58] While CTAB's quaternary headgroup is cationic, its electrostatic interaction efficacy with water is somewhat negated by the presence of its three methyl groups, which sterically hinder the close association between water and the center of the polar headgroup.

The intrinsic density of water plateaus in the middle of the confined water layer ($z > 10$ Å). At the monolayer-water interface, the intrinsic water density does not continue to decay monotonically. There is a local minimum in the intrinsic density at $z \approx 0$ due to the large volume of space excluded by the headgroups. We then observe multiple local maxima in

the region $z < 0$ (the larger of those at $z \approx -4$ Å, with another at $z \approx -6$ Å). This shows that water molecules are able to permeate past the monolayer headgroups, as has been previously observed for SDS monolayers.[55–57,59] This behavior is not seen at the air-water interface, where the water intrinsic density decays monotonically,[2] as shown in SI Figure 5(c) and (d) here. A hard confinement matrix, such as graphite[4] or kaolinite,[8] does not allow permeation of water through the interface to yield the secondary peak. The permeation of water past the monolayer headgroups is probably aided by the bulky CTAB headgroups, whose mutually repulsive Coulombic interactions require mediation by water and counterions to form a stable monolayer. This means that some water molecules come into contact with the hydrophobic tails of the CTAB monolayers. The surface tension of water is sufficient to prevent water molecules from moving significantly past the headgroups at the air-water interface, which suggests that water molecules are unlikely to interact strongly with a neutral substrate, as in the experiments of Dhopatkar and co-workers.[9]

We note that in a symmetric system, shown in Figure 2(a), the two intrinsic densities are identical. There are clear differences between the two intrinsic density profiles calculated for the asymmetric system shown in Figure 2(b). While there is a very modest difference in the main peaks at $z = 2.85$ Å, there are clearer differences at the local minimum at $z = 0$, where the more densely packed monolayer ($A_{\mathrm{CTAB}} = 49$ Å$^2$, orange curve) excludes more water molecules due to the greater volume taken up by the larger number of CTAB headgroups present at the monolayer-water interface. By partitioning the air-water and monolayer-water interfaces (SI Fig. 5(c) and (d)), we see that more water molecules are found in the hydrophobic region 'above' the denser monolayer. This suggests that the denser monolayer more effectively traps water molecules 'above' the monolayer-water interface. The cause of this observation is now probed by examining the intrinsic densities of $N^+$ atoms in the CTAB headgroups (Fig. 3) and the bromide counterions (Fig. 4).

The large, sharp peak in the intrinsic surfactant onium ($N^+$) density profiles shown in Figure 3 confirms that most of the headgroups are found at the water-monolayer interface.

The extreme sharpness of the peak is a consequence of our definition of the intrinsic surface. As expected, we see that the sizes of the main peak and secondary maximum increase with the number of CTAB molecules in the monolayer. Since we do not use the headgroup atoms as predefined anchor points when building the intrinsic surface, we observe a small secondary maximum in the intrinsic onium density at $z \approx -8$ Å (a more negative value of $z$ than the secondary maxima of the water density profiles), which is highlighted in the inset figures in Figure 3. This means that a small percentage of CTAB headgroups are stacked away from the monolayer-water interface at the same lateral position as other CTAB headgroups. This observation can be quantified by integrating the secondary peak. The results confirm that a higher percentage of the headgroups are found stacked away from the monolayer-water interface in denser monolayers. The percentage of headgroups that make the secondary peak in each monolayer are as follows: 9.0% (ML1) and 9.1% (ML2) in SYM49, 7.2% (ML1) and 7.3% (ML2) in SYM52, 7.3% (ML1) and 9.0% (ML2) in ASYM, and 5.6% (ML1) and 9.1% (ML2) in ASYM2.

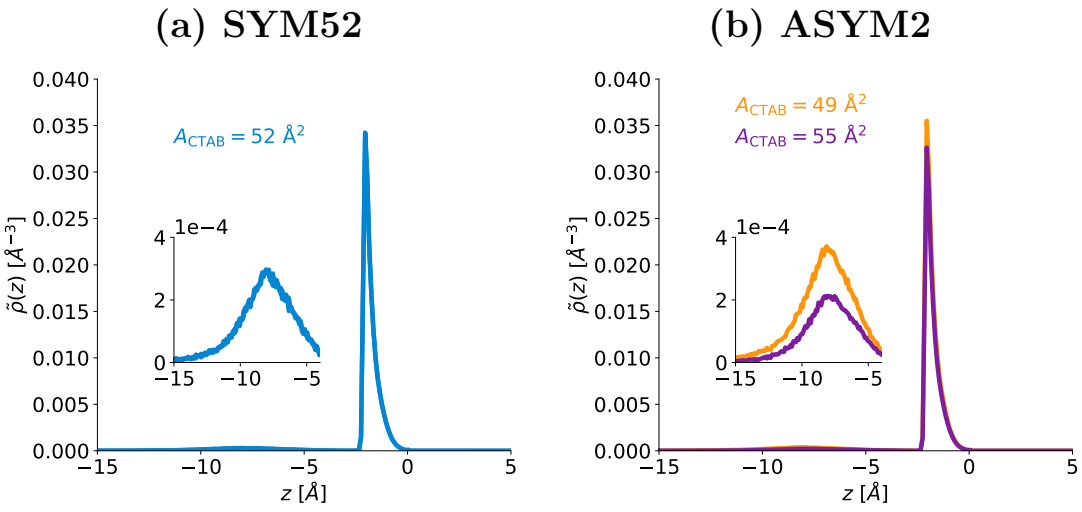


Figure 3: Intrinsic onium ($N^+$) density in (a) SYM52 and (b) ASYM2. Results for the other systems can be found in SI Fig. 6. The inset figures highlight the small, secondary peak in the intrinsic density centered at $z \approx -8$ Å.

The strong peak at $z \approx 4$ Å in intrinsic bromide densities shown in Figure 4 indicates that a large proportion of bromide anions form direct ion pairs with the CTAB headgroups.

There is also significant bromide density at $z < 0$, as for the case of water. The bromide intrinsic densities are identical with respect to the two monolayers in SYM52. However, in ASYM2, a stronger main peak is observed in the case of the more densely packed monolayer (orange curve). More cationic headgroups are available to interact with bromide anions in the denser monolayers. The difference in the bromide intrinsic densities is more apparent than for water, which suggests that bromide out-competes water for interactions with the monolayer headgroups. There is also greater onium density in the range $z < 0$ for the denser monolayer (orange curve). This suggests that denser monolayers trap more water molecules and bromide ions in the $z < 0$ range to mediate the greater repulsion between more densely packed surfactant headgroups. While a majority of the bromide counterions are bound to the cationic headgroups, a significant proportion are not bound (17.0% in SYM49, 17.6% in SYM52, and 18.2% in ASYM2 and SYM52). This partial ion-pair dissociation is observable in the bromide intrinsic density, which remains above zero in the middle of the confined water layer.

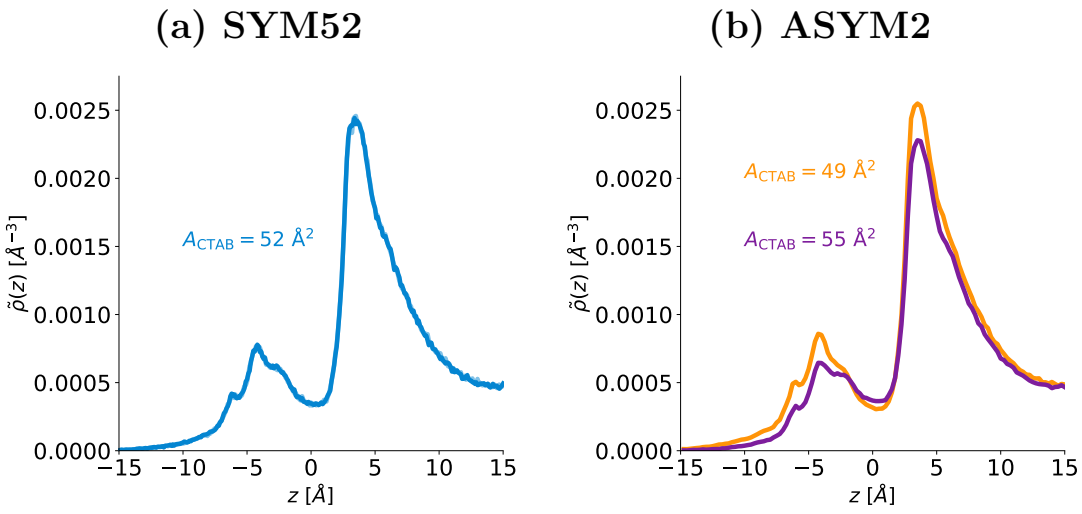


Figure 4: Intrinsic bromide density in (a) SYM52 and (b) ASYM2. Results for the other systems can be found in SI Fig. 7.

## Dynamics of the confined water

The CTAB monolayers greatly affect the dynamics of the confined water. Figure 5 shows the intrinsic van Hove self-correlation function (VHSCF) profiles for the SYM52 and ASYM2 systems. The largest VHSCF values, corresponding to the freest motion, are found in the center of the confined water layers, where water molecules move unhindered by the monolayers. The VHSCF values decrease moving towards the interface with the monolayers, where both steric clashes and attractive intermolecular interactions between water molecules and the surfactant headgroups restrict the movement of water. The VHSCF minimum occurs at $z \approx -4$ Å, behind the monolayer-water interface. SI Figure 5(c) and (d) show that at $z = 0$, a higher proportion of water is found at the air-water interface than at the monolayer-water interface. The water at the air-water interface is able to move freely, unencumbered by the surfactant headgroups. The VHSCF continues to decrease moving towards its global minimum at $z \approx -4$ Å, where more water is found 'above' the monolayer-water interface than at the air-water interface. As well as steric clashes with the monolayers and attractive interactions with the surfactant headgroups, the secondary maximum in the bromide intrinsic densities ($z \approx -4$ Å) suggests hydration complexes formed around bromide ions contribute to the continued decrease in water mobility past the monolayer-water interface. The water molecules in this secondary region are therefore, to a degree, trapped 'above' the monolayer-water interface. The VHSCF plateaus in the middle of the confined water layer ($z \approx 15$ Å), while in MONO, the VHSCF continues to increase until $z \approx 20$ Å (see SI Fig. 8(c)). The motion of the water molecules close to the interface is the same in the MONO system as in the confined systems with the same area per surfactant. However, the motion of the water molecules in the center of the confined water layer is hindered compared to that observed at similar distances from the interface in the unconfined system, which demonstrates that the effects of confinement extend away from the interfaces into the middle of the confined water layer.

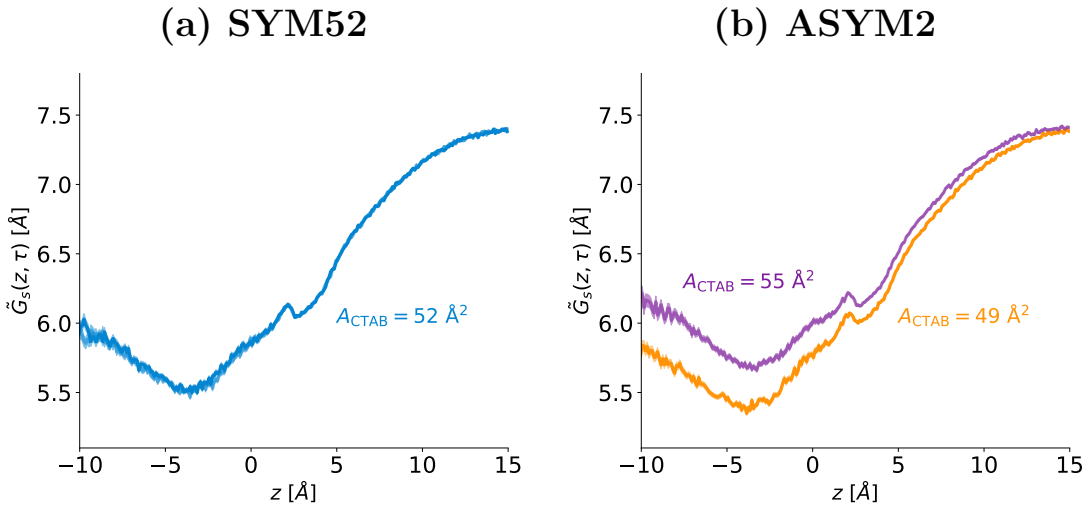


Figure 5: Intrinsic van Hove self-correlation function distributions for water in (a) SYM52 and (b) ASYM2. The results for the other systems can be found in SI Fig. 8.

The symmetric systems show identical VHSCF profiles with respect to both monolayers but a clear difference is seen in the asymmetric systems. The motion of the water molecules is more hindered by the denser monolayer (orange curve in Fig. 5(b)). This difference is not just observed close to the monolayer interface but also extends into the middle of the confined water layer, with the largest difference observed in the water molecules found 'above' the CTAB headgroups.

To link the mobility of the confined water to its underlying structure, we have determined the intrinsic average degree of hydrogen bonding ($\tilde{n}_{\mathrm{HB}}$) throughout the confined water (see SI Fig. 9). The hydrogen bonding structure of water observed in the middle of the confined water layer ($\tilde{n}_{\mathrm{HB}} \approx 3.6$) is disrupted by the monolayers. $\tilde{n}_{\mathrm{HB}}$ falls steeply to a value of $\tilde{n}_{\mathrm{HB}} \approx 2.7$ moving from the middle of the confined layer towards the position of the primary peak in the intrinsic density of water ($z = 2.25$ Å), before remaining approximately constant until $z = 0$, where it again begins to decrease. At $z = -5$ Å, $\tilde{n}_{\mathrm{HB}} \approx 2.3$, retaining approximately 60% of the magnitude of $\tilde{n}_{\mathrm{HB}}$ in the middle of the confined layer. Similar observations have been made for the hydrogen bonding of water at the interface with amorphous silica[60] and polystyrene,[58] whereas water at a hard interface, such as crystalline silica[60] and graphene,[61]

exhibits a single, much sharper drop in the degree of hydrogen bonding. The disruption of water-water hydrogen bonding corresponds to the reduction in water mobility at the monolayer-water interface. A more densely packed monolayer imparts a greater loss of water-water hydrogen bonding (and with it, a greater associated drop in water mobility). As such, non-centrosymmetry clearly emerges in $\tilde{n}_{\mathrm{HB}}$ in the asymmetric systems.

$\tilde{n}_{\mathrm{HB}}$ does not reach its maximum value until the middle of the confined layer and in the unconfined system, $\tilde{n}_{\mathrm{HB}}$ does not recover to its maximum value ($\tilde{n}_{\mathrm{HB}} \approx 3.6$, as for the confined systems) until a distance $\approx 20$ Å from the monolayer-water interface. The distance taken for $\tilde{n}_{\mathrm{HB}}$ to recover to its maximum value is significantly greater than has been previously observed for a range of different interfaces, such as $\alpha$-quartz, $\beta$-cristobalite and amorphous silica[60] (in all three systems, $\tilde{n}_{\mathrm{HB}}$ of bulk water is reached at $\approx 4$ Å from the interface), polystyrene[58] ($\approx 6$ Å), and graphene[61] ($\approx 10$ Å). We expect that the roughness and patchiness of the CTAB monolayers, coupled with the high charge density at the interface, leads to the long-ranged effects on $\tilde{n}_{\mathrm{HB}}$ in the confined water layer seen here.

## Orientation of the confined water layer

The CTAB monolayers impart a large effect on the orientation of water. Figure 6 shows the intrinsic orientational profiles of SYM52 and ASYM2. The order parameters describing the angle between the water bond angle bisection vector and the $z$-axis, $\tilde{\Gamma}^{(1)}(z)$, and its second moment, $\tilde{\Gamma}^{(2)}(z)$, are both shown. There is a peak at $z = 2.25$ Å in $\tilde{\Gamma}^{(1)}(z)$ in all systems, which corresponds to a small local maximum in the VHSCF distributions. In Figure 6(b), a slightly stronger peak in $\tilde{\Gamma}^{(2)}(z)$ is observed for the more densely packed monolayer ($A_{\mathrm{CTAB}} = 49$ Å$^2$). This observation is explored further in the next section. $\tilde{\Gamma}^{(1)}(z)$ decays to zero more quickly than in the unconfined single monolayer system (see SI Fig. 10(c)), showing once more that effects of confinement act throughout the water layer. This observation, in tandem with the reduced VHSCF values for water molecules in the confined layer compared to those at an analogous distance from the MONO surfactant interface with

the same area per surfactant, implies that the forced reordering of water molecules in the middle of the confined system hinders their motion. The $\tilde{\Gamma}^{(2)}(z)$ profiles shown in Figure 6 show that the orientation of water molecules with respect to the interfacial plane is only weakly influenced by interactions with the monolayers.

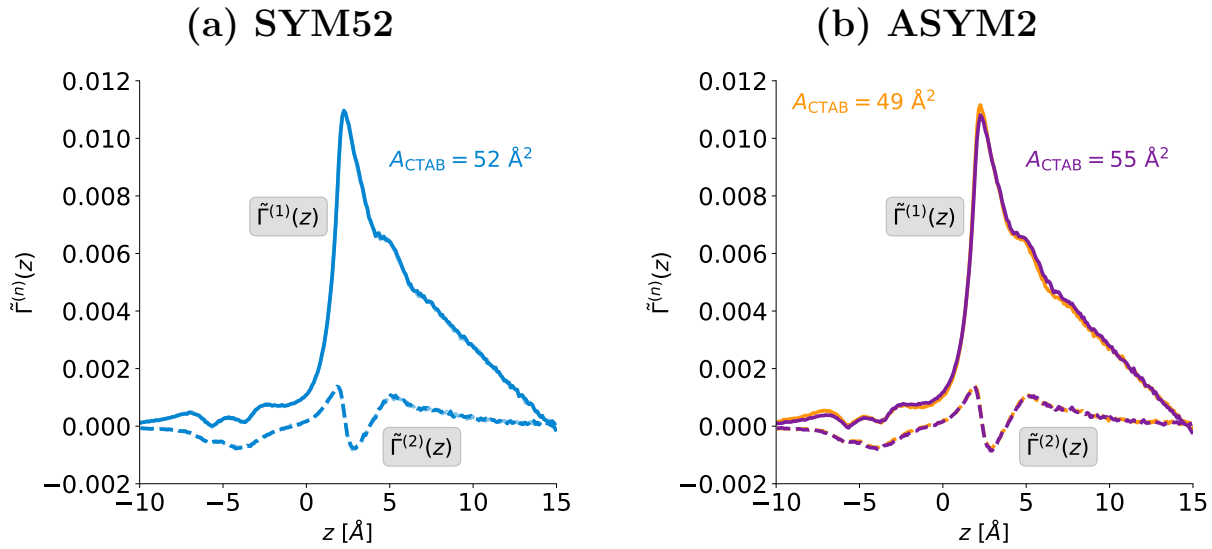


Figure 6: Intrinsic orientational profiles of the confined water in SYM52 (a) and ASYM2 (b). First moment ($\tilde{\Gamma}^{(1)}(z)$, solid lines) and second moment ($\tilde{\Gamma}^{(2)}(z)$, dashed lines). The results for the other systems can be found in SI Fig. 10.

## Effect of local CTAB environment on interfacial water layer

We previously observed that at intrinsic distances corresponding to the main peaks in the density of the confined water layer, the more densely packed monolayer imparts stronger orientational effects (Fig. 6). SI Figure 11 shows the average orientation of water molecules that make up the first hydration shell of CTAB molecules, as a function of the CTAB tilt angle (these angles are depicted in SI Fig. 3); the average orientation of the water molecules in the first hydration layer has a clear dependence on the tilt angle of CTAB molecules with which they interact. Water molecules are still ordered by CTAB molecules that lie parallel to the monolayer-water interface ($\theta_{\text{tilt}}^{\text{CTAB}} = 0°$) to about two-thirds of the extent of those interacting with vertically aligned CTAB molecules ($\theta_{\text{tilt}}^{\text{CTAB}} = 90°$). The large

size of the cationic CTAB headgroup means it can still efficiently order water molecules even when it is not well-ordered. In contrast to the overall orientational ordering observed previously in Figure 6, we now see that on a per-headgroup basis, the less densely packed monolayer imparts a stronger average ordering effect on water molecules in its first hydration shell. This implies that water molecules in the first hydration layer interact with multiple surfactant headgroups simultaneously, with the greater competition for water molecules in the more densely packed monolayers mitigating their overall ordering efficacy. So, although the overall orientational profiles of the ASYM2 system appear quite similar for monolayers of different packing density (see Fig. 6(b)), the contribution per surfactant headgroup on the ordering of water molecules is markedly different between such monolayers. The greater ordering efficacy of the headgroups in the less dense monolayer is counteracted by the greater proportion of the water layer exposed to air at its interface.

To further probe the origins of this observation, we consider the effects of the inter-headgroup coordination number of the CTAB molecules ($n_{\mathrm{N^+,N^+}}$) on the average CTAB tilt angle and the average water dipole tilt angle in Figure 7(a) and (b). $n_{\mathrm{N^+,N^+}}$ acts as a measure of the local CTAB headgroup environment, with lower coordination numbers corresponding to CTAB molecules found at the edge of the patchy domain structures that make up the monolayers, while CTAB molecules with greater coordination lie in the middle of the domains, surrounded by other CTAB molecules. A clear trend is revealed: a more highly coordinated headgroup on average gives rise to a more vertically aligned CTAB molecule. An analogous trend exists in turn for the water molecules: a more highly coordinated CTAB molecule imparts greater orientational ordering on its solvating water molecules. From this we infer that the local ordering imparted on CTAB molecules from neighboring CTAB molecules is in turn transferred to the solvating water molecules. Interestingly, we see that although the average CTAB tilt angle is greater for a more densely packed monolayer, the average water angle is greater at the less densely packed monolayer. We also note that water ordering effects appear to saturate when $n_{\mathrm{N^+,N^+}} = 5$. These two observations imply

that competition for given water molecules between headgroups outweighs the effects of individual CTAB ordering in highly coordinated CTAB environments. Contributions from a single CTAB molecule on the water ordering are greater in a less densely packed monolayer but the greater total number of CTAB molecules in the denser monolayer results in a slightly greater overall ordering of water molecules at the interface (Fig. 6).

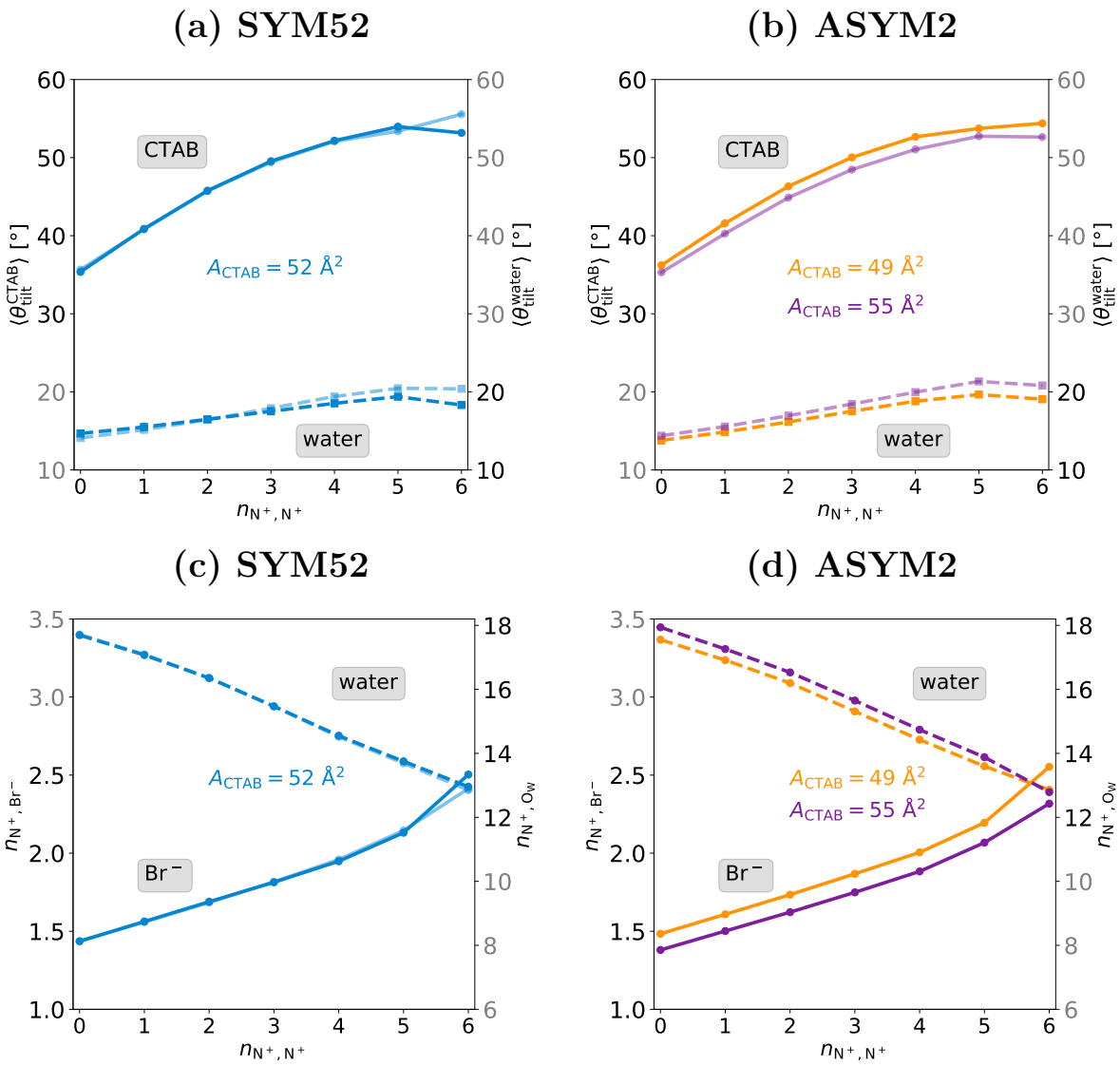


Figure 7: Average water tilt angle ($\theta_{\text{tilt}}^{\text{water}}$, dashed lines) and average CTAB tilt angle ($\theta_{\text{tilt}}^{\text{CTAB}}$, solid lines) as a function of inter-headgroup coordination number in SYM52 (a) and ASYM2 (b). Average headgroup-water coordination number (dashed lines) and average headgroup-bromide coordination number (solid lines) in SYM52 (c) and ASYM2 (d).

Additionally, the coordination numbers of bromide ions and water molecules around

the onium headgroup were calculated as a function of $n_{N^+,N^+}$ (Figs. 7(c) and (d)). Bromide coordination numbers are greater than 1 in all cases and increase with the headgroup-headgroup coordination number. Respectively, this indicates that bromide ions are shared between headgroups and play a key role in bridging between headgroups to maintain the patchy monolayer structures (by counteracting Coulombic repulsion between the cationic headgroups). We see higher water and lower bromide coordination numbers for the lower density monolayer (purple lines in Fig. 7(d)) for all headgroup-headgroup coordination values. More water molecules can surround each CTAB headgroup in a less dense monolayer as there is less competition for space at the interface (fewer counterions and headgroups are present). This presents a quite different picture of water orientation at monolayers of slightly different surface packing density. Since these water molecules face less competition for interactions between different headgroups and counterions in a less dense monolayer, they are more strongly oriented towards each individual headgroup even though there are more water molecules in the first solvation sphere.

# Conclusions

In this work, we have quantified in detail the structure and dynamics of water layers nanoconfined between CTAB monolayers. We have shown that small changes in the packing density of the monolayers lead to significant changes in the properties of water, not only at the interface with the monolayers, but also throughout the entire confined water layer. We have characterized a clear emergence of non-centrosymmetry in water layers confined by two monolayers of subtly different packing densities. Our bespoke intrinsic surface method has resolved the properties of the confined water, fully accounting for the roughness and patchiness of the monolayers themselves. The intrinsic density of water, calculated using the aforementioned intrinsic surface, shows that a greater amount of water is trapped 'above' the CTAB headgroups of a more densely packed monolayer. This population of water 'above' the

interface has recently been indicated experimentally by SFG spectroscopy.[37] Additionally, our intrinsic surface method identified that a significant proportion of CTAB headgroups sit $\approx 8$ Å 'above' the main monolayer-water interface.

We have shown that water trapped 'above' the monolayer-water interface is less mobile than water at the monolayer-water interface itself. We rationalized this observation by partitioning the overall intrinsic water density into monolayer-water and air-water contributions. The effects of the CTAB monolayers on the mobility and hydrogen bonding structure of water extend throughout the entire confined layer. When comparing the confined system to an unconfined analogue, firstly, we see that the mobility of the confined water layer never reaches the mobility of bulk water and secondly, that the water reorientation length scale within the layer is enforced by its confinement. In the unconfined system, the distance from the monolayer-water interface at which no net orientation of water is observed occurs 5 Å further from the monolayer-water interface than in the confined systems.

Even for the small differences in $A_{\mathrm{CTAB}}$ studied in this work, we have observed clear effects on the structure and dynamics of the confined water layer. There is a clear emergence of non-centrosymmetry throughout the entire confined water layer with regard to its structure (especially regarding the amount of water trapped 'above' the headgroups, its intrinsic orientation, and average degree of hydrogen bonding) and dynamics (VHSCF profile) in systems where the water layer is confined by monolayers of subtly different areas per surfactant. We then moved our focus to look at the effects of the CTAB monolayers on water on a per-headgroup basis. This revealed that the less densely packed monolayers both have more water molecules in their first hydration shell but also impart a greater net orientational effect upon them, due to decreased competition effects between headgroups for interactions with the individual water molecules, as indicated by SFG experiments performed by Nguyen *et al.*[32] This is despite the CTAB molecules themselves being less ordered in a less dense monolayer. So while the overall orientational profiles for the asymmetric systems (Fig. 6(b)) look reasonably similar with respect to the two monolayers, they are the product of water

molecules experiencing a different range of physical environments at the two different monolayers. Considering the surfactant packing density dependence of water mobility, hydrogen bonding, and orientation throughout the whole confined water layer provides atomistic insight into the interesting SFG spectroscopy results recently reported by Dhopatkar *et al.*[9]

## Acknowledgement

We thank Theodora Mears for proofreading the manuscript. R.M.Z., F.F. and C.D.L. acknowledge the supportive research environment of the EPSRC Centre for Doctoral Training in Cross-Disciplinary Approaches to Non-Equilibrium Systems (CANES, No. EP/L015854/1). Through C.D.L.'s membership within the UK HPC Materials Chemistry Consortium, which is funded by the Office of Science and Technology through the EPSRC High End Computing Programme (Grant No. EP/L000202, EP/R029431), the use of ARCHER, the UK National Supercomputing Service (http://www.archer.ac.uk) and the UK Materials and Molecular Modelling Hub (MMM Hub), which is partially funded by EPSRC (EP/P020194/1), was made possible for the molecular dynamics simulations presented in this work.

## Supporting Information Available

Details of the simulated systems not presented in the main article are available in the supporting information. This material is available free of charge via the Internet at `http://pubs.acs.org/`.

## References

(1) Chakraborty, S.; Kumar, H.; Dasgupta, C.; Maiti, P. K. Confined Water: Structure, Dynamics, and Thermodynamics. *Acc. Chem. Res.* **2017**, *50*, 2139–2146.

(2) Du, Q.; Freysz, E.; Shen, Y. R. Surface Vibrational Spectroscopic Studies of Hydrogen Bonding and Hydrophobicity. *Science* **1994**, *264*, 826–8.

(3) Zichi, D. A.; Rossky, P. J. The Equilibrium Solvation Structure for the Solvent-Separated Hydrophobic Bond. *J. Chem. Phys.* **1985**, *83*, 797–808.

(4) Jinesh, K. B.; Frenken, J. W. M. Experimental Evidence for Ice Formation at Room Temperature. *Phys. Rev. Lett.* **2008**, *101*, 036101.

(5) Granick, S. Motions and Relaxations of Confined Liquids. *Science* **1991**, *253*, 1374–1379.

(6) Lorenz, C. D.; Lane, J. M. D.; Chandross, M.; Stevens, M. J.; Grest, G. S. Molecular Dynamics Simulations of Water Confined between Matched Pairs of Hydrophobic and Hydrophilic Self-Assembled Monolayers. *Langmuir* **2009**, *25*, 4535–4542.

(7) Lorenz, C. D.; Chandross, M.; Lane, J. M. D.; Grest, G. S. Nanotribology of Water Confined between Hydrophilic Alkylsilane Self-Assembled Monolayers. *Model. Simul. Mater. Sci. Eng.* **2010**, *18*, 034005.

(8) Haria, N. R.; Grest, G. S.; Lorenz, C. D. Viscosity of Nanoconfined Water between Hydroxyl Basal Surfaces of Kaolinite: Classical Simulation Results. *J. Phys. Chem. C* **2013**, *117*, 6096–6104.

(9) Dhopatkar, N.; Defante, A. P.; Dhinojwala, A. Ice-Like Water Supports Hydration Forces and Eases Sliding Friction. *Sci. Adv.* **2016**, *2*, e1600763–e1600763.

(10) Bampoulis, P.; Sotthewes, K.; Dollekamp, E.; Poelsema, B. Water Confined in Two-Dimensions: Fundamentals and Applications. *Surf. Sci. Rep.* **2018**, *73*, 233–264.

(11) Peschel, G.; Adlfinger, K. H. Viscosity Anomalies in Liquid Surface Zones: IV. The Apparent Viscosity of Water in Thin Layers Adjacent to Hydroxylated Fused Silica Surfaces. *J. Colloid Interface Sci.* **1970**, *34*, 505–510.

(12) Horn, R. G.; Smith, D. T.; Haller, W. Surface Forces and Viscosity of Water Measured between Silica Sheets. *Chem. Phys. Lett.* **1989**, *162*, 404–408.

(13) Kim, H. I.; Kushmerick, J. G.; Houston, J. E.; Bunker, B. C. Viscous Interphase Water Adjacent to Oligo(ethylene glycol)-Terminated Monolayers. *Langmuir* **2003**, *19*, 9271–9275.

(14) Major, R. C.; Houston, J. E.; McGrath, M. J.; Siepmann, J. I. S.; Zhu, X.-Y. Viscous Water Meniscus under Nanoconfinement. *Phys. Rev. Lett.* **2006**, *96*, 177803.

(15) Klein, J.; Kumacheva, E. Simple Liquids Confined to Molecularly Thin Layers. I. Confinement-Induced Liquid-to-Solid Phase Transitions. *J. Chem. Phys.* **1998**, *108*, 6996.

(16) Raviv, U.; Laurat, P.; Klein, J. Fluidity of Water Confined to Subnanometre Films. *Nature* **2001**, *413*, 51–54.

(17) Klein, J.; Raviv, U.; Perkin, S.; Kampf, N.; Chai, L.; Giasson, S. Fluidity of Water and of Hydrated Ions Confined between Solid Surfaces to Molecularly Thin Films. *J. Phys. Condens. Matter* **2004**, *16*, S5437.

(18) De Simone, A.; Dodson, G. G.; Verma, C. S.; Zagari, A.; Fraternali, F. Prion and Water: Tight and Dynamical Hydration Sites Have a Key Role in Structural Stability. *Proc. Natl. Acad. Sci. U.S.A.* **2005**, *102*, 7535–7540.

(19) Yuan, S.; Ma, L.; Zhang, X.; Zheng, L. Molecular Dynamics Studies on Monolayer of Cetyltrimethylammonium Bromide Surfactant Formed at the Air/Water Interface. *Colloids Surf. A* **2006**, *289*, 1–9.

(20) Gragson, D. E.; McCarty, B. M.; Richmond, G. L. Ordering of Interfacial Water Molecules at the Charged Air/Water Interface Observed by Vibrational Sum Frequency Generation. *J. Am. Chem. Soc.* **1997**, *119*, 6144–6152.

(21) Cantat, L.; Cohen-Addad, S.; Elias, F.; Graner, F.; Höhler, R.; Pitois, O.; Rouyer, F.; Saint-Jalmes, A. *Foams: Structure and Dynamics*; Oxford University Press: Oxford, UK, 2013.

(22) Binks, B. B. *Modern Aspects of Emulsion Science*; Royal Society of Chemistry: Cambridge, UK, 1998.

(23) Schramm, L. L. *Surfactants: Fundamentals and Applications in the Petroleum Industry*; Cambridge University Press: Cambridge, UK, 2000.

(24) Myers, D. *Surfactant Science and Technology,* 3rd edition; John Wiley & Sons: Hoboken, NJ, 2005.

(25) Paria, S.; Khilar, K. C. Microemulsion-Based Media as Novel Drug Delivery Systems. *Adv. Drug Delivery Rev.* **2000**, *45*, 89–121.

(26) Lawrence, M. J.; Rees, G. D. A Review on Experimental Studies of Surfactant Adsorption at the Hydrophilic Solid-Water Interface. *Adv. Colloid Interface Sci.* **2004**, *110*, 75–95.

(27) Rabinow, B. E. Nanosuspensions in Drug Delivery. *Nat. Rev. Drug Discovery* **2004**, *3*, 785–796.

(28) Mishra, B.; Patel, B. B.; Tiwari, S. Colloidal Nanocarriers: A Review on Formulation Technology, Types and Applications Toward Targeted Drug Delivery. *Nanomed. Nanotechnol. Bio. Med.* **2010**, *6*, 9–24.

(29) Cohen, L.; Martin, M.; Soto, F.; Trujillo, F.; Sanchez, E. The Effect of Counterions of Linear Alkylbenzene Sulfonate on Skin Compatibility. *J. Surfactants Deterg.* **2016**, *19*, 219–222.

(30) Banipal, T. S.; Kaur, H.; Kaur, A.; Banipal, P. K. Effect of Tartarate and Citrate Based

Food Additives on the Micellar Properties of Sodium Dodecylsulfate for Prospective Use as Food Emulsifier. *Food Chem.* **2016**, *190*, 599–606.

(31) Kumar, S.; Mandal, A. Studies on Interfacial Behavior and Wettability Change Phenomena by Ionic and Nonionic Surfactants in Presence of Alkalis and Salt for Enhanced Oil Recovery. *Appl. Surf. Sci.* **2016**, *372*, 42–51.

(32) Nguyen, K. T.; Nguyen, A. V.; Evans, G. M. Interfacial Water Structure at Surfactant Concentrations below and above the Critical Micelle Concentration as Revealed by Sum Frequency Generation Vibrational Spectroscopy. *J. Phys. Chem C* **2015**, *119*, 15477–15481.

(33) Pan, X.; Yang, F.; Chen, S.; Zhu, X.; Wang, C. Cooperative Effects of ZwitterionicIonic Surfactant Mixtures on the Interfacial Water Structure Revealed by Sum Frequency Generation Vibrational Spectroscopy. *Langmuir* **2018**, *34*, 5273–5278.

(34) Yazhgur, P.; Vierros, S.; Hannoy, D.; Sammalkorpi, M.; Salonen, A. Surfactant Interactions and Organization at the Gas-Water Interface (CTAB with Added Salt). *Langmuir* **2018**, *34*, 1855–1864.

(35) Bonn, M.; Nagata, Y.; Backus, E. H. G. Molecular Structure and Dynamics of Water at the Water-Air Interface Studied with Surface-Specific Vibrational Spectroscopy. *Angew. Chem.* **2015**, *54*, 5560–5576.

(36) Nihonyanagi, S.; Yamaguchi, S.; Tahara, T. Ultrafast Dynamics at Water Interfaces Studied by Vibrational Sum Frequency Generation Spectroscopy. *Chem. Rev.* **2017**, *117*, 10665–10693.

(37) Dutta, C.; Mammetkuliyev, M.; Benderskii, A. V. Re-Orientation of Water Molecules in Response to Surface Charge at Surfactant Interfaces. *J. Chem. Phys.* **2019**, *151*, 034703.

(38) Pal, S.; Bagchi, B.; Balasubramanian, S. Hydration Layer of a Cationic Micelle, C 10 TAB: Structure, Rigidity, Slow Reorientation, Hydrogen Bond Lifetime, and Solvation Dynamics. *J. Phys. Chem. B* **2005**, *109*, 12879–12890.

(39) Mackerell Jr., A. D.; Feig, M.; Brooks, C. L. Extending the Treatment of Backbone Energetics in Protein Force Fields: Limitations of Gas-Phase Quantum Mechanics in Reproducing Protein Conformational Distributions in Molecular Dynamics Simulations. *J. Comput. Chem.* **2004**, *25*, 1400–1415.

(40) Vanommeslaeghe, K.; Hatcher, E.; Acharya, C.; Kundu, S.; Zhong, S.; Shim, J.; Darian, E.; Guvench, O.; Lopes, P.; Vorobyov, I.; Mackerell Jr., A. D. CHARMM General Force Field: A Force Field for Druglike Molecules Compatible with the CHARMM All-Atom Additive Biological Force Fields. *J. Comput. Chem.* **2010**, *31*, 671–690.

(41) Jorgensen, W. L.; Chandrasekhar, J.; Madura, J. D.; Impey, R. W.; Klein, M. L. Comparison of Simple Potential Functions for Simulating Liquid Water. *J. Chem. Phys.* **1983**, *79*, 926–935.

(42) Vanommeslaeghe, K.; Hatcher, E.; Acharya, C.; Kundu, S.; Zhong, S.; Shim, J.; Darian, E.; Guvench, O.; Lopes, P.; Vorobyov, I.; Mackerell, A. D. CHARMM general force field: A force field for drug-like molecules compatible with the CHARMM all-atom additive biological force fields. *J. Comput. Chem.* **2009**, *31*, 671–690.

(43) Klauda, J. B.; Venable, R. M.; Freites, J. A.; O'Connor, J. W.; Tobias, D. J.; Mondragon-Ramirez, C.; Vorobyov, I.; MacKerell Jr., A. D.; Pastor, R. W. Update of the CHARMM All-Atom Additive Force Field for Lipids: Validation on Six Lipid Types. *J. Phys. Chem. B* **2010**, *114*, 7830–7843.

(44) Haria, N. R.; Lorenz, C. D. Ion Exclusion and Electrokinetic Effects Resulting from Electro-osmotic Flow of Salt Solutions in Charged Silica Nanopores. *Phys. Chem. Chem. Phys.* **2012**, *14*, 5935–5944.

(45) Pascal, T. A.; Goddard, W. A.; Jung, Y. Entropy and the driving force for the filling of carbon nanotubes with water. *Proc. Natl. Acad. Sci. U.S.A.* **2011**, *108*, 11794–11798.

(46) Horinek, D.; Mamatkulov, S. I.; Netz, R. R. Rational Design of Ion Force Fields Based on Thermodynamic Solvation Properties. *J. Chem. Phys.* **2009**, *130*, 124507.

(47) Martìnez, L.; Andrade, R.; Birgin, E. G.; Martìnez, J. M. PACKMOL: A Package for Building Initial Configurations for Molecular Dynamics Simulations. *J. Comput. Chem.* **2009**, *30*, 2157–2164.

(48) Plimpton, S. Fast Parallel Algorithms for Short-Range Molecular Dynamics. *J. Comput. Phys.* **1995**, *117*, 1–19.

(49) Shinoda, W.; Shiga, M.; Mikami, M. Rapid Estimation of Elastic Constants by Molecular Dynamics Simulation Under Constant Stress. *Phys. Rev. B* **2004**, *69*, 134103.

(50) Ryckaert, J. P.; Ciccotti, G.; Berendsen, H. J. Numerical Integration of the Cartesian Equations of Motion of a System with Constraints: Molecular Dynamics of n-Alkanes. *J. Comput. Phys.* **1977**, *23*, 327–341.

(51) Michaud-Agrawal, N.; Denning, E. J.; Woolf, T. B.; Beckstein, O. MDAnalysis: A Toolkit for the Analysis of Molecular Dynamics Simulations. *J. Comput. Chem.* **2011**, *32*, 2319–2327.

(52) Humphrey, W.; Dalke, A.; Schulten, K. VMD: Visual Molecular Dynamics. *J. Mol. Graph.* **1996**, *14*, 33–38.

(53) Allen, D. T.; Lorenz, C. D. A Novel Method for Constructing Continuous Intrinsic Surfaces of Nanoparticles. *J. Mol. Model.* **2017**, *23*, 219.

(54) Pártay, L. B.; Hantal, G.; Jedlovszky, P.; Vincze, Á.; Horvai, G. A New Method for Determining the Interfacial Molecules and Characterizing the Surface Roughness in

Computer Simulations. Application to the Liquid-Vapor Interface of Water. *J. Comput. Chem.* **2008**, *29*, 945–956.

(55) Martínez, H.; Chacón, E.; Tarazona, P.; Bresme, F. The Intrinsic Interfacial Structure of Ionic Surfactant Monolayers at Water-Oil and Water-Vapour Interfaces. *Proc. Royal Soc. Lond. A* **2011**, *467*, 1939–1958.

(56) Allen, D. T.; Saaka, Y.; Pardo, L. C.; Lawrence, M. J.; Lorenz, C. D. Specific Effects of Monovalent Counter Ions on the Structural and Interfacial Properties of Dodecyl Sulphate Monolayers. *Phys. Chem. Chem. Phys.* **2016**, *18*, 30394–30406.

(57) Allen, D. T.; Damestani, N.; Saaka, Y.; Lawrence, M. J.; Lorenz, C. D. Interaction of Testosterone-Based Compounds with Dodecyl Sulphate Monolayers at the Air-Water Interface. *Phys. Chem. Chem. Phys.* **2018**, *20*, 8790–8801.

(58) Bekele, S.; Tsige, M. Characterizing the Hydrophobicity of Surfaces Using the Dynamics of Interfacial Water Molecules. *J. Phys. Chem. C* **2018**, *122*, 9020.

(59) Saaka, Y.; Allen, D. T.; Luangwitchajaroen, Y.; Shao, Y.; Campbell, R. A.; Lorenz, C. D.; Lawrence, M. J. Towards Optimised Drug Delivery: Structure and Composition of Testosterone Enanthate in Sodium Dodecyl Sulfate Monolayers. *Soft Matter* **2018**, *14*, 3135–3150.

(60) Lorenz, C. D.; Tsige, M.; Rempe, S. B.; Chandross, M.; Stevens, M. J.; Grest, G. S. Simulation Study of the Silicon Oxide and Water Interface. *J. Comput. Theor. Nanos.* **2010**, *7*, 2586–2601.

(61) Gordillo, M. C.; Marti, J. Water on Graphene Surfaces. *J. Phys. Condens. Matter* **2010**, *22*, 284111.

# Graphical TOC Entry